Experimental and Three-Dimensional Finite Element Study of Scratch Test of Polymers at Large Deformations

J. L. Bucaille

E. Felder
e-mail: eric.felder@ensmp.fr

Centre for Materials Forming,
UMR 7635 du CNRS,
Ecole des Mines de Paris,
06904 Sophia Antipolis,
France

G. Hochstetter
Essilor International,
94106 Saint Maur des Fossés,
France

An experimental and numerical study of the scratch test on polymers near their surface is presented. The elastoplastic response of three polymers is compared during scratch tests at large deformations: polycarbonate, a thermosetting polymer and a sol-gel hard coating composed of a hybrid matrix (thermosetting polymer-mineral) reinforced with oxide nanoparticles. The experiments were performed using a nanoindenter with a conical diamond tip having an included angle of 30 deg and a spherical radius of 600 nm. The observations obtained revealed that thermosetting polymers have a larger elastic recovery and a higher hardness than polycarbonate. The origin of this difference in scratch resistance was investigated with numerical modelling of the scratch test in three dimensions. Starting from results obtained by Bucaille (J. Mat. Sci., **37***, pp. 3999–4011, 2002) using an inverse analysis of the indentation test, the mechanical behavior of polymers is modeled with Young's modulus for the elastic part and with the G'sell-Jonas' law with an exponential strain hardening for the viscoplastic part. The strain hardening coefficient is the main characteristic parameter differentiating the three studied polymers. Its value is equal to 0.5, 4.5, and 35, for polycarbonate, the thermosetting polymer and the reinforced thermosetting polymer, respectively. Firstly, simulations reveals that plastic strains are higher in scratch tests than in indentation tests, and that the magnitude of the plastic strains decreases as the strain hardening increases. For scratching on polycarbonate and for a penetration depth of 0.5 μm of the indenter mentioned above, the representative strain is equal to 124%. Secondly, in agreement with experimental results, numerical modeling shows that an increase in the strain hardening coefficient reduces the penetration depth of the indenter into the material and decreases the depth of the residual groove, which means an improvement in the scratch resistance.* [DOI: 10.1115/1.1645535]

1 Introduction

Organic materials are often used in the ophtalmic industry because of their low density, their relative toughness and their high elastic recovery. But their hardness and scratch resistance is far low compared to those of mineral materials, which degrades their optic and esthetic properties. In order to improve their scratch resistance, a sol-gel hard coating (1–3 μm) is deposited on the surface. The resistance to scratches of such a layer is due to its mechanical properties, for which the measurement is impossible with classical tests (tension or compression). Instrumented scratch is then a good alternative to study such materials. On the other hand, the mechanical understanding of such a test is intricate and still in progress.

Experimental studies of scratch on polymers have been carried out to investigate the formation of wear particles [1]. The transition of the ductile to brittle behavior depends on the attack angle of the indenter and on the size of the volume strained by the indenter [2–5]). The attack angle, β, (or the included angle, θ, for a conical indenter) is related to the representative strain in indentation or scratch through the following relation suggested by Johnson [6] (Fig. 1):

$$\varepsilon_r = 0.2 \tan \beta = 0.2 \cot \theta. \quad (1)$$

In fact, the value of the proportionality coefficient depends on the kind of test (scratch or Indentation [7]), so this definition strictly speaking is not satisfactory, and may be misleading [8]. But it is well established that the lower the β, the lower the plastic strains. Thus, for small values of β, the plastic deformation is small compared to the total deformation, and the scratch is mainly elastic. This behavior is called ''ironing'' [9]. The material sinks-in in front of the indenter, the contact between the indenter and the material occurs at the front and at the rear and the residual depth of the groove is low compared to the penetration depth under loading [10,11]. All of these behaviors observed in scratch tests on polymers are well identified, but the relationship with the mechanical properties of the materials is not well understood. The objective of this study is to utilize finite element simulations to show that the scratch resistance of a polymer, or the transition between the elastic behavior and ductile ploughing, depends greatly on strain hardening.

Three dimensional finite element analysis of materials due to scratching is recent. Tangena et al. [12] and Kral and Komvopoulos [13] have performed finite element simulations on elastoplastic materials under sliding contact conditions. In these cases, the representative strain defined with Eq. 1 is less than one percent and elements are not severely deformed. For larger attack of angle β, elements beneath the indenter are extremely distorted. To overcome this numerical difficulty a new mesh must be created during the calculation. Numerical techniques may be used to simulate scratch tests at large deformations: Bucaille et al. [11] and Subhash and Zhang [14] have used a code utilizing of an automatic remeshing procedure and an explicit code, respectively.

In a previous work, Bucaille et al. [15] and Bucaille [16] studied three polymers and identified their mechanical behavior, i.e. the true stress-true strain curve, using an inverse analysis of the indentation test with two different indenter shapes. For these poly-

Contributed by the Tribology Division for publication in the ASME JOURNAL OF TRIBOLOGY. Manuscript received by the Tribology Division August 29, 2002; revised manuscript received June 24, 2003. Associate Editor: Q. J. Wang.

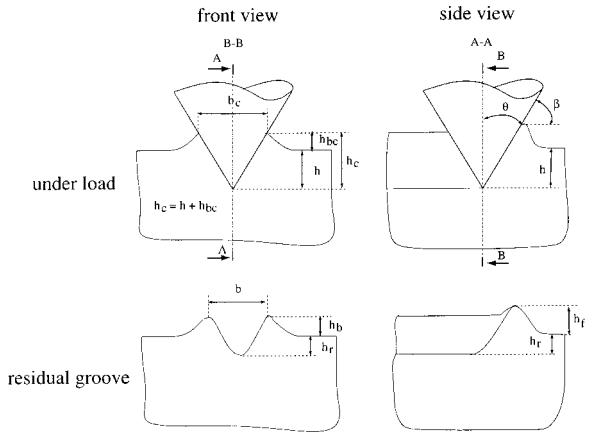

Fig. 1 Geometrical parameters measured during a scratch test

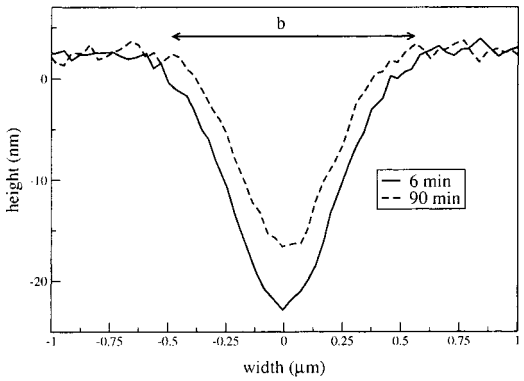

Fig. 2 Experimental profile of the scratch groove of oa10 measured with the tip of the nanoindenter used as a profilometer 6 min and 90 min after the scratch test, $v=2\ \mu$m/s, $W=1$ mN. The residual depth and the scratch width continue to decrease several minutes after the scratch test.

mers, scratch experiments are compared with numerical results using a commercially available software. The effect of the rheology is analyzed and more specifically the effect of strain hardening of each polymer, on their behavior in scratch and indentation tests.

2 Experimental and Modeling Procedures

2.1 Nanomechanical Testing. Three polymers were considered in the present study: two bulk materials, polycarbonate (PC) and CR39®, and a varnish of 3 μm thick, oa10. Polycarbonate is a thermoplastic polymer obtained by injection molding. CR39® (diethylene glycol-bis allyl carbonate) is a thermosetting resin obtained by casting and heated for 20 hours at 80°C. The monomer is an allyl resin which not only polymerizes but also cross-links which results in a thermoset plastic. The varnish is composed of an hybrid matrix (thermosetting-mineral) reinforced with nanoparticules of silica (with a typical size about 10–15 nanometers). The precursor of the hybrid matrix, the glymo, leads to a crosslinked material having polymeric and mineral segments, due to the Si-O-Si bonds. The polymer segments induce a time dependent mechanical behavior: this is the reason why, in the following part of this study, the hard coating will be assimilate to a thermosetting polymer reinforced by nanoparticules of silica, but one should remain that is a simplified description of a complex material. Its function is to protect substrates from scratches. This varnish was deposited on the CR39® by dip coating. These materials are considered as homogeneous and thus, have constant mechanical properties through their thickness.

The scratch experiments were performed using a NanoindenterII® from MTS. The load and displacement resolutions of the system are 75 nN and 0.1 nm, respectively. The indenter is first displaced tangentially with a small normal load, $W=0.02$ mN, to record the profile of the initial surface of the sample. This linear scan produces no permanent groove in the material. The indenter is dept perpendicularly to the surface, and the normal load is increased to the specified value, W. The normal force W is then maintained constant, and the tip is displaced tangentially with a scratch speed, v, over a scratching distance of 20 μm. The average values of the normal force, the tangential force, F_t and the penetration depth, h, are measured over the scratching distance. The apparent coefficient of friction was calculated as the ratio of the tangential force to the normal force:

$$\mu_0=\frac{F_t}{W}. \tag{2}$$

Finally, the indenter is displaced with a normal load $W=0.02$ mN, perpendicular to the scratch direction across the bottom of the groove. The profile of the residual scratch is recorded which yields the scratch width, b, and the residual height, h_r, 90 minutes after the scratch test (Fig. 1). For polycarbonate, b is considered to be the distance between the peaks of the lateral pile-ups. For CR39® and oa10, no pile-up was observed and thus, b is measured as shown in Fig. 2.

Scratch hardness is defined as the ratio of the normal force to the projected residual contact area. For materials having a low modulus to flow stress ratio (E/σ), the material sinks-in in front of the indenter and the elastic recovery is large, whereas for high values, the behavior is mainly plastic and a pile-up in front of the indenter occurs. Thus, the elastic recovery and the pile-up of the material around the tip are potential sources of error in calculating scratch hardness. As the amount of elastic recovery can not be measured using the nanoindenterII, nominal scratch hardness is defined by assuming that the contact only occurs over the front of the indenter as in the case of metals, on a half disc:

$$H_{s1/2}=\frac{8W}{\pi b^2} \tag{3}$$

Scratch tests were performed on polycarbonate, CR39® and oa10 with an axisymmetric diamond cone having an included angle of 30 deg and a tip radius of 600 nm. Considering the definitions of the representative plastic strain imposed by a sharp indenter given by Johnson [6] and Bucaille et al. [15], the representative strain resulting from indentation by a conical indenter with a spherical tip may be written as follows:

$$\varepsilon_r=0.2\frac{h}{a}. \tag{4}$$

Normal forces were chosen in order that the penetration of the indenter in all materials reaches at least 500 nm, which corresponds to the maximum value of the attack angle, β, of 60 deg. For the penetration depths considered in the scratch experiments, ε_r is at least 16%. Three normal forces were chosen for polycarbonate and CR39® and one for oa10 (Table 1). In preliminary nanoindentation experiments on oa10 using a pointed Berkovich tip, both hardness and Young's modulus were constant for penetration depths lower than 600 nm. This shows that the influence

Table 1 Normal loads used for scratch experiments for $v=2\ \mu$m/s

	W (mN)		
PC, CR39®	0.49	0.73	0.98
oa10		0.98	

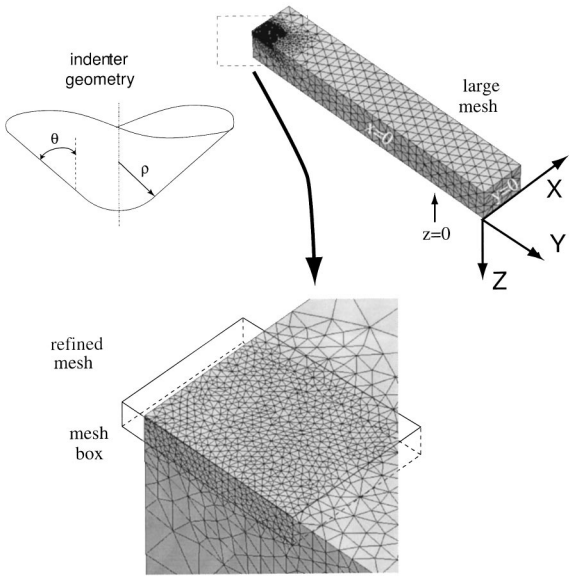

Fig. 3 Three-dimensional view of the mesh used for the simulation of scratch. The mesh box placed near the indenter tip contains small sized elements and moves with the indenter along the *Y* axis. The indenter is a cone of semiapical angle θ=30 deg with a tip radius of 600 nm.

of the substrate can be neglected in further mechanical analysis. Normal forces were limited to 0.98 mN to avoid delamination of the coating or formation of brittle fractures. Optical observations of the residual grooves revealed no evident cracks. This indicates that, at this scale of observation, the behavior of the three polymers is viscoelastic or ductile. For all the samples, the scratch speed, v, was equal to 2 μm/s.

2.2 Simulation of Scratch and Indentation. Scratching simulations were modeled using the Forge3® implicit code using an automatic remeshing procedure. The domain is a right-angled parallelepiped. Figure 3 shows half of the finite-element mesh corresponding to the region $x \geqslant 0$, with the plane x=0 a symmetry plane. The displacement of the mesh in the other directions was prevented by two planes $y=0$ and $z=0$ which are also considered as symmetry planes. The size of the domain was chosen so that boundary effects do not influence the results (Table 2, [16]). The indenter used in the scratch experiments was considered rigid and modeled as an axisymmetric cone with an included angle θ=30 deg and a spherical tip of 600 nm radius. The displacement of the indenter was along the *y*-axis with a scratch speed of 2 μm/s, its penetration depth was constant, and was equal to the values reported in Table 3. Elements of the domain were three-dimensional meshes with four-node tetrahedra. Far from the indenter, elements had a typical length of about 1 μm. With the Forge3® software, parallepiped boxes were used, and where the mesh was refined, 20 nodes were at least in contact with the indenter on the generatrix in the plane $x=0$. For example, a scratch simulation on polycarbonate required 11,000 nodes and 45,000 elements, about 35 hours of CPU time, and a remeshing procedure every five increments. For each time increment, normal and tangential forces

Table 2 Size of the domain and typical size of elements near the indenter in the scratch simulations

Maximum Penetration (μm)	Width (μm)	Length (μm)	Height (μm)	Size of Elements near the Indenter (μm)
1	8	50	10	0.04

Table 3 Penetration depths used for scratch simulations for v=2 μm/s

	h (nm)		
PC, CR39®	500	750	1000
oa10		500	

were computed. A post processing procedure gave the average of several geometrical parameters such as the scratch width, b, the pile-up height (for polycarbonate), h_b, and the residual depth, h_r (Fig. 1). For CR39® and oa10, the material sinks-in near the indenter, as observed in scratch experiments. However, the transition between the groove and the nominal surface of the material is not as marked and can not be determined as shown in Fig. 2. For simulation, the scratch width is defined as the contact width between the indenter and the mesh under loading, and scratch hardness is computed considering a half-disc of contact (Eq. 3).

The indentation test was modeled with Forge2®, a two dimensional axisymmetric finite element code. A two-dimensional rectangular mesh incorporating six-nodes elements was constructed. Elements had a length of 0.04 μm near the indenter and of 3 μm far from the indenter. The rigid indenter was modeled as an axisymmetric cone with an included angle θ=30 deg and a spherical tip of 600 nm radius. During loading, the ratio of the indenter speed, $\dot{h}$, to the penetration depth, h, was maintained constant and equal to 0.049 s^{-1}. More details concerning simulation of the indentation tests are given in [15].

2.3 Modeling of the Rheology of the Polymers. All polymers were considered as homogeneous and bulk materials. Their rheological and tribological properties are summarized in Table 4. The elastic behavior was modeled by a linear law with two constant parameters: Poisson's ratio, ν and Young's modulus, E, i.e., the viscoelasticity is neglected. This strong assumption will be discussed later. E was determined in indentation with the slope at the beginning of the unloading curve via a method described in [17] (Table 4). Poisson's ratio of polycarbonate and CR39® were obtained in compression [16]. The value of ν for the varnish was assumed to be the same as for CR39® (Table 4). The yield condition was given by the von Mises yield criterion and the flow stress was described by a simplified G'sell-Jonas law [18]:

$$\sigma = K e^{h_g \varepsilon^2} \dot{\varepsilon}^m, \tag{5}$$

where K is a strength coefficient, h_g is the strain hardening coefficient, and m the sensitivity to the strain rate. This law was first determined for uniaxial tests and the exponential term, $e^{h_g \varepsilon^2}$, models the strain hardening of polymers at large deformations due to the extension of macromolecules of polymers. Bisilliat [19] showed that this strain hardening begins earlier and is larger in tension than in compression. These three parameters were deter-

Table 4 Coefficient of friction, elastic and viscoplastic properties of polycarbonate, CR39® and oa10 used in the simulation of scratch and indentation tests. Friction coefficient, μ, was obtained by measurements of apparent friction coefficient in scratch [16]; ν was measured in compression [16]; E was obtained in indentation [17]; m, K, and h_g were determined using an inverse analysis of indentation [15,16].

	PC	CR39®	oa10
μ	0.3	0.3	0.2
m	0.053	0.078	0.033
K (MPa·s^{-m})	102	145	138
h_g	0.5	4.5	35
E (GPa)	2.4	2.1	3.19
ν	0.35	0.4	0.4

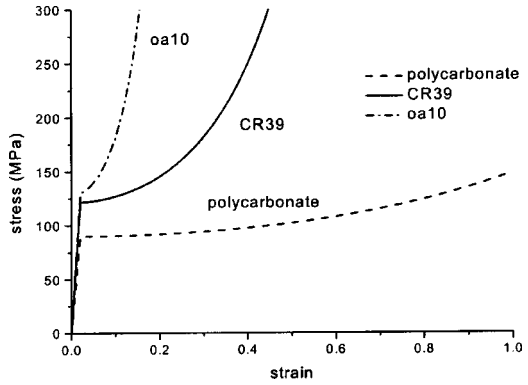

Fig. 4 True stress-true strain curves of polycarbonate, CR39® and oa10, obtained by an inverse analysis in indentation by Bucaille [16] for $\dot{\varepsilon}=10^{-1}\,s^{-1}$. These results show that CR39® and oa10 have a larger strain hardening than polycarbonate.

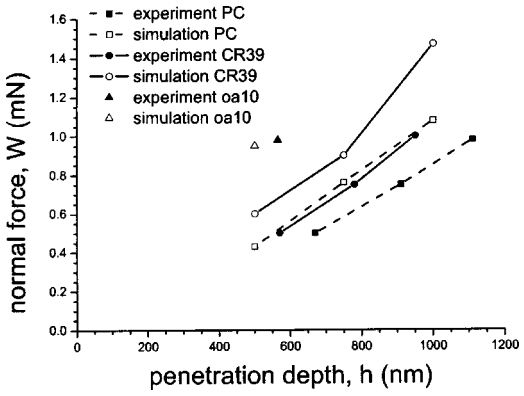

Fig. 5 Normal forces of polycarbonate, CR39® and oa10 as a function of the penetration depth of the indenter. Comparison between experimental and numerical results of scratch tests.

mined by an inverse method, based on the interpretation of the force-penetration curves in indentation with two indenter shapes [15] (Table 4, Fig. 4).

Bucaille et al. [15] considered that this strain hardening also occurs during an indentation test. Macromolecules of polymer are locally extended in the directions normal to the indenter speed. This can explain why the strain hardening exponent in indentation is similar to the value in compression. Figure 4 shows that the yield stress is similar for oa10 and CR39®, and 37% higher than for polycarbonate. But the most noticeable effect of the nature of the material is on the strain hardening exponent: for polycarbonate, the value of h_g is about nine times lower than for the thermosetting polymer, CR39®. This effect is even larger when nanoparticles are added to a thermoset matrix. Interestingly, this evolution of the strain hardening exponent can be well correlated with the existence of chemical crosslink in the CR39®, compared to polycarbonate, or with the colloid addition in the sol-gel hard coating compared to the CR39®. This remains a phenomenological description of the behavior of these materials. Nevertheless, this phenomenological model seems well adapted for the purpose of this paper, that is focused on the major differences existing between the three analyzed materials, particularly for the large deformations.

Friction at the interface between the indenter and the material for both simulation of indentation and scratch tests was modeled with a Coulomb coefficient of friction, μ. Its value was determined with measurements of the apparent coefficient of friction, μ_0, for sliding of a sphere on polycarbonate, CR39®, and oa10 [16]. This coefficient is assumed to be the same in indentation and scratch, and to be independent of strain and strain rate (Table 4).

3 Results and Discussion

Experimental and numerical results of scratch tests on polycarbonate, CR39®, and oa10 are plotted in Figs. 5, 6, and 7. In the first section, measurements obtained with the nanoindenter are considered. These results are then compared with those of the numerical simulations. For a similar penetration depth, the influence of the modeling of the rheology on the behavior observed and computed in the scratch test is discussed for the three polymers. Finally, the behavior of polycarbonate and CR39® during indentation and scratch tests is compared.

3.1 Results of Scratch Experiments. Figure 5 shows the variation of the normal load with the penetration depth of polycarbonate and CR39® measured during scratch experiments. For oa10, only a normal force of 0.96 mN was chosen, which corresponds to a penetration depth of 560 nm. For polycarbonate and CR39® the penetration depth increases with increasing normal force. For a normal force of 0.96 mN, the penetration depth of oa10 is 2 times and 1.7 times lower than for polycarbonate and CR39® respectively, indicating that the varnish is much harder than the two bulk materials. This is confirmed by the measurements of hardness (Fig. 6). The hardness of oa10 is thus 6 times higher than that of polycarbonate and CR39®. Figure 6 also shows the variation of the hardness with the penetration depth.

Measurements of hardness are prone to several errors, and a particularly bad estimation of the contact radius may induce a large error in the computation of the scratch hardness. It was

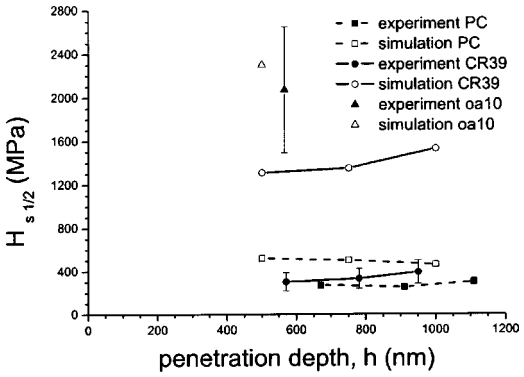

Fig. 6 Depth dependence of scratch hardness of polycarbonate, CR39® and oa10 computed with a half disc of contact. Comparison between simulations and experiments of scratch tests. Error bars are due to the uncertainties in the experimental measurement of the scratch width.

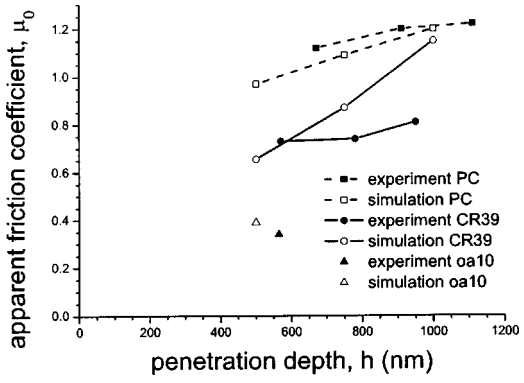

Fig. 7 Apparent coefficient of friction of polycarbonate, CR39® and oa10 measured during scratch experiments and simulations as a function of the penetration depth

observed on polycarbonate grooves that the heights of the pile-ups are not the same on each side of the groove. This was attributed to the shape of the indenter. The fabrication of such axisymmetric indenters is very complicated, and the actual indenter is not perfectly axisymmetric. This implies a difference of at least 10% in the value of the scratch width, depending on the direction of the scratch. The second source of error is due to the viscoelasticity of polymers: for oa10, the residual scratch width measured 6 minutes and 90 minutes after the scratch test decreases about 18% (Fig. 2). Within this period, the scratch width of polycarbonate remained quite constant. Although most of the viscoelastic recovery happens for all materials in the first seconds after the scratch (Gauthier et al. [10]) and can not be observed with the nanoindenter, the error in the estimation of the scratch width due to viscoelasticity was only considered for the thermosetting polymers and added to the 10% due to the actual shape of the indenter.

Nevertheless, the trend for $H_{s1/2}$ is to increase with increasing penetration depth for polycarbonate and CR39® although for all the penetration depths considered here, the attack angle is equal to 60°. This indicates that, for such penetration depths, the spherical part of the indenter has a strong influence on the behavior of the material. For polycarbonate, the increase of hardness is about 13%, while it reaches 23% for CR39®. This confirms that the variation of the representative strain with penetration depth in a scratch test is better described by the ratio h/a than the attack angle. According to Eq. 4, this ratio increases about 30% for both polycarbonate and CR39® as W increases from 0.48 mN to 0.96 mN. In addition, this increase in hardness with increasing h indicates that the flow stress increases as the strain in the material increases and that it is more marked for CR39®.

Figure 7 shows the variation in the apparent friction coefficient of polycarbonate, CR39® and oa10 with the penetration depth. The apparent coefficient of friction increases as the penetration depth increases. The apparent coefficient of friction can be divided in the sum of the ploughing component, μ_p, and the friction component, μ_a [20]:

$$\mu_0 = \mu_p + \mu_a . \tag{6}$$

The friction component depends on the Coulomb coefficient friction μ. By assuming that the contact pressure is constant at the interface between the indenter and the material, the factors μ_p and μ_a do not depend on the nature of the material itself, but on the penetration depth of the indenter into the material and on the magnitude of the elastic recovery at the rear of the indenter [20]. Even if μ is smaller for oa10 than for polycarbonate and CR39®, the low values of μ_0 for oa10 are then interpreted as the consequence of the large elastic recovery at the rear of the indenter, this phenomena being smaller for CR39® and even smaller for polycarbonate. These results show that the nature of the material has important consequences on the response in a scratch test; and that this effect is larger than the influence of the penetration depth. In the next section, these experimental results are compared with those computed in numerical simulation of scratch tests with the rheological model adopted in Sec. 2.3.

3.2 Comparison Between Experiment and Simulation. Results of the simulations show the same trends as those observed during scratch experiments, i.e., an increase of $H_{s1/2}$ and μ_0 as the penetration depth increases, except for variation in hardness of polycarbonate which decreases about 16%. This is attributed to the fact that the groove width is a bad estimation of the contact area. From the simulations, the real projected contact area, A, between the indenter and the material was determined. Scratch hardness ($H_s = W/A$) can thus be calculated without uncertainties in the value of the contact area at the rear of the indenter or the difference between the measured scratch width and the real contact width. For polycarbonate, H_s increases with increasing penetration depth. This confirms that the deformation level increases with increasing penetration depth. Figure 5 shows that normal forces computed from the simulations are about 30% higher than those computed during scratch experiments. The rheological model adopted is relatively simple and, in particular, does not take into account the strain softening of polycarbonate at small strains, the dependence of the hydrostatic pressure, nor the anisotropy due to the macromolecular orientation of the material at high strains. As the difference between simulation and experiment is relatively constant with increasing penetration depth, this error may be attributed to an overestimation of the strength coefficient, K, or Young's modulus, E. Furthermore, the behavior of a material during a scratch is much more complex than during an indentation test. The material is highly compressed in front of the indenter and in tension at the rear. Indeed, Bucaille and Felder [7] showed that the representative strain is about 1.7 higher during a scratch test than during indentation. The behavior obtained in indentation is then extrapolated, which also may explain why computed normal forces are higher.

Table 5 Apparent coefficient of friction, scratch hardness computed with the entire projected contact area, $H_s = W/A$, and elastic recovery in the groove computed in the simulations, $v = 2\ \mu$m/s and $h = 500$ nm

Material	Polycarbonate	CR39®	oa10
μ_0	0.93	0.62	0.37
H_s (MPa)	405	969	1387
$1 - h_r/h$ (%)	16	40	49

The variation of μ_0 with increasing h is larger than what was determined experimentally, however, values are of the same order of magnitude (Fig. 7). Figure 6 shows that the normal hardnesses computed from the simulations are higher than hardnesses measured during scratch experiments. This is especially marked for CR39® where $H_{s1/2}$ is three times higher in the simulations, although the difference in the normal force is much lower (Fig. 5). As explained in the previous section, the width of the residual groove continues to decrease several minutes after scratching, which implies an error in the estimation in the frontal contact area and thus the hardness.

Inherent differences in this type of complex test and simulation of these materials remain. However, finite element simulations showed, as observed during scratch experiments, that the apparent friction coefficient is higher for polycarbonate and is smaller for CR39® and finally for oa10, and that the hardest material is oa10 following by CR39® and then polycarbonate. Although the rheological law adopted to model polymers is relatively simple and does not take into account some aspects of the physical properties of these materials, the software reproduces well, at a first approximation, their behaviors during a scratch test.

3.3 Influence of the Rheology on the Scratching Behavior. In this section, the scratch behavior of the three polymers for a penetration depth equal to 500 nm computed in the simulations, and for a normal force equal to 0.98 mN for the experiments with a scratch speed equal to 2 μm/s is compared. Based on finite element results, the origin of the evolution of hardness and apparent friction coefficient for the polymers is investigated.

For a similar nominal penetration depth, the apparent coefficient of friction varies from 0.93 for polycarbonate to 0.37 for oa10 (Table 5). This is due to the elastic recovery of the rear face of the indenter, which is larger for the thermosetting resins (Sec. 3.1). In the present section, finite element simulations bring new information which helps interpret the experimental measurements. Even if nominal penetration depths are equal ($h = 0.5\ \mu$m) for all the polymers studied, the contact height, h_c (Fig. 1), depends strongly on the scratched material. Figure 8 shows that for $h = 0.5\ \mu$m, the contact height computed varies from 0.35 μm for oa10 to 0.7 μm for polycarbonate. For this indenter, the transition height between the spherical and conical part is equal to 0.3 μm. The ploughing component, μ_p, of μ_0 is then strongly modified by this difference in the contact height. By considering only the fron-

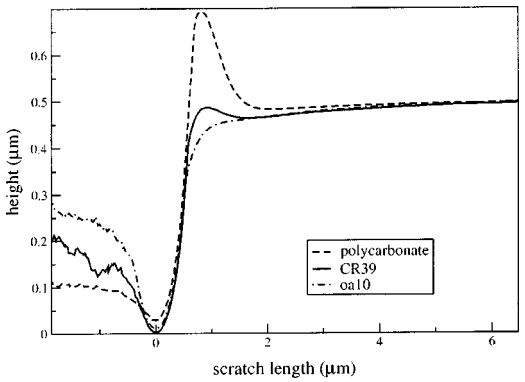

Fig. 8 Scratch profile computed in simulation in the plane $x=0$ for polycarbonate, CR39® and oa10, $v=2$ μm/s, $h=500$ nm. For polycarbonate a pile-up is created at the front of the indenter. For oa10, the material sinks-in and the elastic recovery at the back of the indenter is more than 50 percent.

tal part of the contact between the indenter and the material and by using analytical models of μ_0 given in [20], μ_p varies from 0.58 (oa10) to 0.82 (PC). For oa10, this value is higher than the measured value. However, the contact with the rear of the indenter decreases this ploughing part. Thus, without friction and for a complete elastic recovery μ_0 tends to 0. Values of μ_0 can then be related to the magnitude of the elastic recovery of the material. Figure 9 shows that for polycarbonate, the projected rear contact area represents only 24% of the contact in front of the indenter. For oa10, frontal and lateral contact radius are smaller than those for polycarbonate and the projected contact area is a complete disc. Numerical modelling has shown that the contact pressures in the front and on the rear back of the indenter are similar, so the value of μ_0 for oa10 corresponds to the adhesive part of friction which acts on both frontal and back parts. The elastic recovery occuring at the rear face of the indenter during a scratch test can be divided into an instantaneous recovery and a viscoelastic recovery. The first part is modeled in simulations by Young's modulus. The viscoelastic behavior has not been modeled and has only a small effect on the rear of contact; on the other hand, it is responsible for the delayed elastic recovery which explains the higher values of $1-h_r/h$ measured during scratch experiments (Tables 5 and 6). The elastic recovery, $1-h_r/h$, measured in the bottom of the groove is 54%, 93%, and 97% for polycarbonate, CR39® and oa10, respectively (Table 6). Figure 8 and optical observations (Fig. 10) show that scratching on polycarbonate is plastic, with a large pile-up formation in front and on the sides of the groove. The ratio of the height of the lateral pile-up, h_b, to the penetration depth, h, is about 23% in both simulation and experiment. The behavior of the thermosetting polymers is nearly elastic, no pile-up on the side of the scratch is observed during experiments and simulations (Fig. 2). The same variation was computed in the finite element simulation (Table 5). One must note the particular behavior of CR39® in front of the indenter in Fig. 8. There is a small pile-up of the material, however the contact boundary is located below the nominal surface of the material.

The polymers were modeled with a large strain hardening. Modeling of the scratch test show similar behaviors as those observed in the experiments. A simulation of the scratch test on polycarbonate, with a saturation of the strain hardening at a plastic strain of 1.5 ($\sigma\sim280$ MPa), shows that the material flow is totally different: the frontal pile-up degenerates to chip formation (Fig. 11). Additional simulations confirmed that this behavior is even more marked as the strain hardening is saturated for smaller strains. Plastic strains are much higher and the elastic recovery is almost zero. Experimentally, such damage is not observed. This shows the importance of correctly modelling the rheology of polycarbonate and taking into account the strain hardening. On the other hand, viscoelastic effects principally contribute to the elastic recovery at the rear of the indenter.

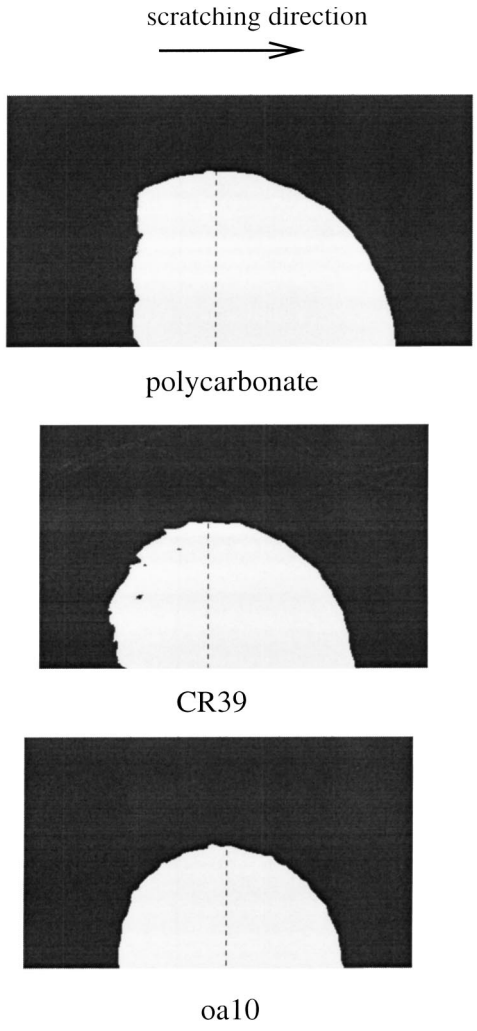

Fig. 9 Top view of the contact area between the indenter and the material computed in simulation of scratch tests, $h=500$ nm, $v=2$ μm/s. For oa10, the elastic recovery at the back of the indenter is complete.

3.4 Plastic Strains and Representative Strain in Indentation and Scratch Tests. The behavior of polymers can be better understood by plotting the evolution of the ratio of the plastic strain, ε_p, to the elastic strain, ε_e, as a function of the plastic strain (Fig. 12). The elastic strain is the ratio between the flow stress, σ, and Young's modulus, E. The flow stress is computed with Eq. (5). For polycarbonate, and for plastic strains lower than 1 (Fig. 4), the flow stress is almost constant, and the elastic strain

Table 6 Apparent coefficient of friction, scratch hardness computed with the frontal contact area, $H_{s1/2}$, penetration depth and elastic recovery in the groove measured during scratch experiments, $v=2$ μm/s and $W=0.98$ mN

Material	Polycarbonate	CR39®	oa10
μ_0	1.22	0.82	0.34
$H_{s1/2}$ (MPa)	312	380	2062
h (nm)	1100	950	505
$1-h_r/h$ (%)	54	93	97

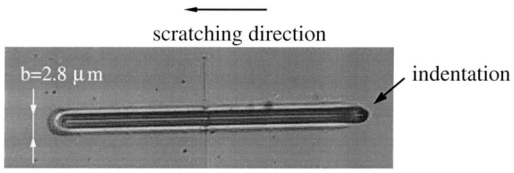

Fig. 10 Optical view of the residual groove of polycarbonate performed with the nanoindenter for $W=0.98$ mN and $v=2$ μm/s. During the indentation step (right side), polycarbonate sinks-in; during scratch test pile-ups are visible on the side of the groove and at the end of the groove.

is also constant so the deformation of the material is mainly plastic. For higher plastic strains, the consequence of the strain hardening is that the elastic strain becomes higher than the plastic strain. The behavior of the material becomes more and more elastic. This explains why during indentation the material sinks-in under the indenter: plastic strains at the limit of the contact do not exceed 0.4, while in scratch test these values reach the value of one, which represents the maximum value of $\varepsilon_p/\varepsilon_e=12$, and then form a lateral pile-up (Figs. 12 and 13). The same behaviors were observed in the scratch experiments (Fig. 10). For CR39® and oa10, the behavior is similar, however the ratio of $\varepsilon_p/\varepsilon_e$ does not reach values higher than 2; with respect to the elastic strains, the plastic strains are not sufficient to form a pile-up.

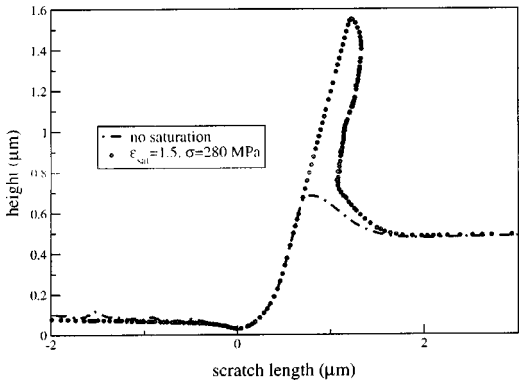

Fig. 11 Scratch profile of polycarbonate computed in simulation for two different rheological behaviors introduced in the software. If von Mises stresses (σ=280 MPa) are saturated for plastic strains higher than 1.5, a chip is produced in front of the indenter.

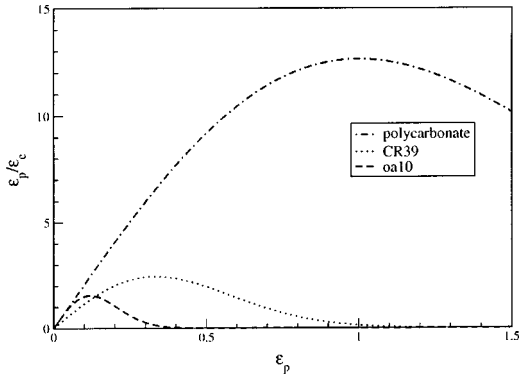

Fig. 12 Ratio of the plastic strain to the elastic strain as a function of the plastic strain, for polycarbonate, CR39® and oa10, $\dot{\varepsilon}=10\ s^{-1}$. For polycarbonate, plastic strains may be more than ten times higher than elastic strains, this explains the formation of piles-up.

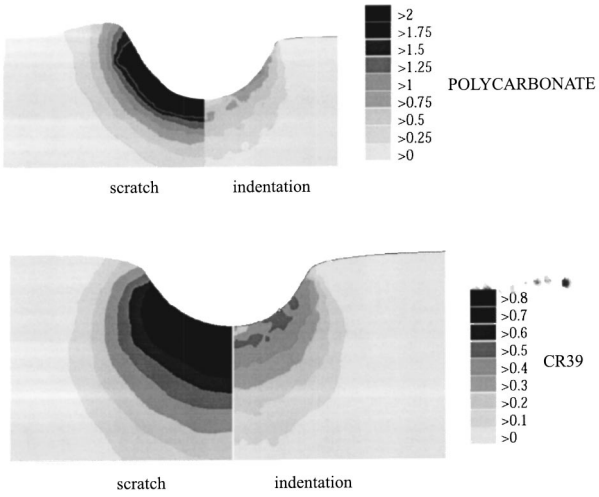

Fig. 13 Maps of equivalent plastic strains computed in simulation of scratch and indentation tests for polycarbonate and CR39®, $h=0.5$ μm; indentation $v/h=0.49\ s^{-1}$; scratch $v=0.2$ μm/s. Plastic strains are higher during scratch tests than during indentation tests. The behavior of polycarbonate is more plastic than for CR39®: plastic strains are higher and a lateral pile-up is created (scratch).

Previous discussions have demonstrated that the hardnesses, $H_{s1/2}$, measured after scratch experiments are not reliable and that H_s computed in finite element simulations by considering the whole contact area represents a mean value of the contact pressure that the indenter exerts on the material. By the following discussion it will be demonstrated that the representative strain in a scratch test, defined in the spirit of Tabor [21], depends strongly on the rheology of the material. While for plastic materials, the ratio between hardness and representative flow stress, H_s/σ, is equal to 3 [21], Gauthier et al. [10] consider for PMMA a value of 1.84. In a first approximation, this ratio is assumed to be the same for the three polymers studied here. Values of hardness, H_s, are indicated in Table 5 for a scratch speed $v=2$ μm/s. The strain rate in a scratch test is defined by Briscoe et al. [2] as the ratio of the scratch speed, v, to the scratch width, b. $\dot{\varepsilon}$ is then equal approximately to 1 s^{-1}. The representative strain is deduced from Eq. 5 with coefficients in Table 4. The representative strain is equal to 0.22, 0.54, and 1.24 for oa10, CR39® and polycarbonate, respectively. These values are in agreement with the values indicated on the map of equivalent plastic strains in Fig. 13. Bucaille and Felder [7] modeled scratch tests on elastoplastic materials without strain hardening and proposed a relation of the representative strain:

$$\varepsilon_r=0.151\log\left(\frac{E}{\sigma}\cot\theta\right)\cot\theta \tag{7}$$

By replacing $\cot\theta$ with h/a, the representative plastic strain is then equal to 0.042, 0.046, and 0.14 for oa10, CR39® and polycarbonate, respectively. Values are lower than those calculated above. This difference is explained as follows: the range of plastic deformation of polymers is much higher than for other materials. Compared to metals, the strain hardening of polymers is higher and starts for larger plastic strains. Equation (7) is thus not adaptable for such materials and a factor equal to at least 5 must be introduced. Most of the authors have used the same definition in indentation and scratch tests for the representative strain, as in Tabor [21]. The difference in the behavior between scratch and indentation tests, observed for instance for polycarbonate, implies that material flow around the indenter is not similar. In a scratch test, the material is first compressed in front of the indenter, and is

in tension at the rear back of the indenter. The magnitude of these phenomena depends on the mean deformation imposed by the indenter and on the material. For polycarbonate, plastic strains computed in simulation are greater than 2 during a scratch, and do not exceed 1 during indentation (Fig. 13). For CR39®, maximum values of plastic strains are 2 times greater during scratch tests than during indentation tests (Fig. 13). This confirms, to a first approximation, the ratio of 1.7 between the representative strain in scratch and indentation tests for elastic-perfectly plastic materials suggested by Bucaille and Felder [7]. By increasing the penetration depth of the indenter during indentation, plastic strains increase and reach constant values, but they are not high enough to reach those computed during a scratch. This confirms, as already explained in Sec. 3.2, that the stress-strain curves used to model the behavior during scratch are an extrapolation of the behavior determined from indentation.

4 Conclusions

Scratching of three polymers by a sharp indenter was studied: a thermoplastic polymer (polycarbonate), a thermosetting polymer (CR39®), and a sol-gel hard coating reinforced with oxide nanoparticles (oa10). The aim of this work was to state more precisely the relations between scratch behavior and rheology at high strains. Previous work [16] on the same materials using an inverse analysis of the indentation test with two indenter geometries showed that the main difference between these three materials is their strain hardening behavior. The strain hardening exponent was found to be 0.5, 4.5, and 35 for polycarbonate, CR39®, and oa10, respectively.

Scratch experiments using a nanoindenter were conducted on these three materials, with a conical indenter having an included angle equal to 30 deg and a spherical tip of 600 nm radius, for three normal loads. Finite element simulations were also performed with the same indenter and the rheology identified during indentation [16]. Both experiments and simulations showed an increase in hardness and apparent friction coefficient with increasing penetration depth. Numerical modelling also reproduced the same classification of the three polymers observed during scratch experiments, i.e., friction coefficient is lower for the thermosetting resins, and hardness increases in the following order: PC, CR39® and oa10. Simulation and experiment showed that polycarbonate has a plastic behavior characterized by the formation of pile-ups in front of the indenter and on the sides of the residual groove. Scratch experiments exhibited a large viscoelastic recovery on the bottom of the residual groove, which can reach 90% for the thermosetting resins. Although such large viscoelastic behaviors were not modeled, ductile ploughing and elastic deformation, for polycarbonate and thermosetting resins, respectively, were reproduced in the simulations.

The origin of these behaviors is strongly linked to the strain hardening of the polymers. The increase in the strain hardening firstly increases the elastic recovery at the rear face of the indenter, which decreases the apparent friction coefficient; and secondly increases the hardness of the material. This indicates a fundamental notion, specific to polymers: in order to reduce the residual groove after a scratch test, the material must be hard and elastic at the same time. Here oa10 is more than three times harder than polycarbonate, and its elastic recovery is twice as high. These two types of behavior have been successfully modeled with the exponential strain hardening of the G'sell Jonas' law. Consequently, the higher the strain hardening, the higher the scratch resistance.

For strain hardening materials, plastic strains do not depend only on the geometry of the indenter. Plastic strains are higher in scratch tests than in indentation tests. Maps of equivalent plastic strains have revealed that plastic strains are higher for polycarbonate than for the thermosetting resins. This shows that the relationship suggested by Johnson [6] for indentation tests on metals can not be used to define the representative strain in a scratch test on polymers. The piling-up/sinking-in transition is linked to the ratio of plastic strain to elastic strain. Plastic strains ten times higher than elastic strains are thus sufficient to form a pile-up.

Acknowledgment

Essilor INTL Coatings Research and Development is acknowledged for its interest for the results and for its financial support for part of this work. We would like to address our thanks to A. Jimenez who performed the scratch experiments.

References

[1] Adams, M. J., Allan, A., Briscoe, B. J., Doyle, P. J., Gorman, D. M., and Johnson, S. A., 2001, "An Experimental Study of the Nano-Scratch Behavior of Poly(methyl methacrylate)," Wear, **251**, pp. 1579–1583.
[2] Briscoe, B. J., Evans, P. D., Pelillo, E., and Sinha, S. K., 1996, "Scratching Maps for Polymers," Wear, **200**, pp. 137–147.
[3] Stuart, B. H., and Briscoe, B. J., 1996, "Scratch Hardness Studies of Pol(ether ether ketone)," Polymer, **37**(17), pp. 3819–3824.
[4] Bertrand Lambotte, P., 2001, "Nano-Indentation, Scratching and Atomic Force Microscopy for Evaluating the Mar Resistance of Automotive Clearcoats: Study of the Ductile Scratches," Thin Solid Films, **306-312**, pp. 398–399.
[5] Lu, W., and Komvopoulos, K., 2001, "Nanomechanical and Nanotribological Properties of Carbon, Chromium, and Titanium Carbide Ultrathin Films," ASME J. Tribol., **123**, pp. 717–724.
[6] Johnson, K. L., 1970, "The Correlation of Indentation Experiments," J. Mech. Phys. Solids, **18**, pp. 115–126.
[7] Bucaille, J. L., and Felder, E., 2002, "Finite Element Analysis of Deformation During Indentation and Scratch Tests on Elastic Perfectly-Plastic Materials," Philos. Mag. A, **82**(10), pp. 2003–2012.
[8] Chaudhri, M. M., 1998, "Subsurface Strain Distribution Around Vickers Hardness Indentations in Annealed Polycrystalline Copper," Acta Mater., **46**(9), pp. 3047–3056.
[9] Briscoe, B. J., Pelillo, E., Ragazzi, F., and Sinha, S. K., 1998, "Scratch Deformation of Methanol Plastized Poly(methylmethacrylate) Surfaces," *Polymer*, **39**(11), pp. 2161–2168.
[10] Gauthier, C., Lafaye, S., and Schirrer, R., 2001, "Elastic Recovery of a Scratch in a Polymeric Surface: Experiments and Analysis," Tribol. Int., **34**, pp. 469–479.
[11] Bucaille, J. L., Felder, E., and Hochstetter, G., 2001, "Mechanical Analysis of the Scratch Test on Elastic Perfectly-Plastic Materials With the Three Dimensional Finite Element Modeling," Wear, **249**(5–6), pp. 422–432.
[12] Tangena, A. G., Franklin, S., and Franse, J., 1989, "Scratch Tests on Hard Layers," in *Mechanics of Coatings*, D. Dowson, C. M. Taylor, and M. Godet, eds., pp. 169–174.
[13] Kral, E. R., and Komvopoulos, K., 1997, "Three-Dimensional Finite Element Analysis of Subsurface Stress and Strain Fields Due to Sliding Contact on an Elastic-Plastic Layered Medium," ASME J. Tribol., **119**, pp. 332–341.
[14] Suhbash, G., and Zhang, W., 2002, "Investigation of the Overall Friction Coefficient in Single-Pass Scratch Test," Wear, **252**, pp. 123–134.
[15] Bucaille, J. L., Felder, E., and Hochstetter, G., 2002, "Identification of the Viscoplastic Behavior of a Polycarbonate Based on Experiments and Numerical Modeling of the Nanoindentation Test," J. Mater. Sci., **37**, pp. 3999–4011.
[16] Bucaille, J. L., 2001, "Simulation Numérique de l'Indentation et de la Rayure des Verres Organiques," Ph.D. thesis, Ecole Nationale Supérieure des Mines de Paris.
[17] Hochstetter, G., Jimenez, A., and Loubet, J.-L., 1999, "Strain Rate Effects on Hardness of Glassy Polymers in the Nanoscale Range. Comparison Between Quasi-Static and Continuous Stiffness Measurements," J. Macromol. Sci., Phys., **B38**(5–6), pp. 681–692.
[18] G'Sell, C., 1995, *Introduction à la Mécanique des Polymères*, Chapter Lois de Comportement Mécanique des Polymères Solides, C. G'Sell and J. M. Haudin, eds., Institut National Polytechnique de Lorraine, pp. 141–168.
[19] Bisilliat, M. L., 1997, "Comportement mécanique d'un polycarbonate à grande vitesse de sollicitation. Etude expérimentale et simulation," Ph.D thesis, Ecole Nationale Supérieure des Mines de Paris.
[20] Goddard, J., and Wilman, H., 1962, "A Theory of Friction and Wear During the Abrasion of Metals," Wear, **5**, pp. 114–135.
[21] Tabor, D., 1951, *The Hardness of Metals*, Clarendon Press, Oxford.